THE JOURNAL OF PHYSICAL CHEMISTRY A
A JOURNAL OF THE AMERICAN CHEMICAL SOCIETY

pubs.acs.org/JPCA

Article

# Quantum Chemical Study on the Evolution of Sulfur Functional Groups during Char Burnout

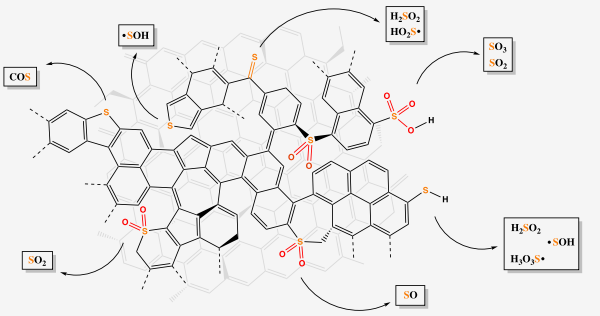
Bastian Schnieder,* Rochus Schmid, and Christof Hättig

Cite This: *J. Phys. Chem. A* 2025, 129, 3300−3314

Read Online

ACCESS | Metrics & More | Article Recommendations

**ABSTRACT:** The oxy-fuel combustion of biochar connected with carbon capture, storage, and utilization technologies is an environmentally beneficial alternative for the replacement of fossil fuels. Biochar itself consists of porously stacked layers of hydrocarbons containing several heteroatoms, such as oxygen, nitrogen, and sulfur. At present, only limited information on the combustion mechanisms for oxygen and nitrogen functionalities is available in the literature; specific information on the combustion mechanisms of sulfur-containing groups (SFGs) is lacking. In this study, we present electronic structure calculations to uncover the mechanisms of the initial oxidation reactions of SFGs. Furthermore, it is examined if the reaction mechanisms remain similar or change with increasing system size. For this purpose, we apply an automatized workflow combining reactive molecular dynamics simulations with static electronic structure calculations at different levels of theory. The results show that terminal groups such as thiols, sulfonic acids, thioketones, and *S*,*S*-dioxides follow similar reaction pathways. These SFGs are all gradually oxidized before they eventually are eliminated as $SO_x(H_y)$ species from the carbon framework. Embedded thiophenes follow somewhat different reaction pathways that lead to the elimination of HOS· radicals or carbonyl sulfide (COS), depending on the system size. For the found oxidation channels, we report reaction and activation energies and rate constants that can be used to improve comprehensive kinetic models for the combustion of sulfur-containing biochar as a biomass-based renewable energy source.




## INTRODUCTION

In terms of sustainability, fossil fuel-based electricity generation technologies contribute significantly to global warming. In light of climate change, it is desirable to reduce emissions of greenhouse gases and pollutants into the Earth's atmosphere. One promising technology that has attracted global attention in the past decade is the combustion of fossil fuels in an oxy-fuel atmosphere, which allows to produce a concentrated stream of flue gases consisting primarily of carbon dioxide ($CO_2$). The combination of oxy-fuel technologies with carbon capture, utilization, and storage (CCUS) technologies[1,2] is an innovative concept of global importance, preventing or at least reducing the release of environmentally harmful greenhouse gases into the atmosphere. While CCUS strategies have the potential to efficiently contribute to reducing the carbon intensity of global energy production, they simultaneously pose several challenges. The successful implementation of CCUS requires integration into existing infrastructure and energy systems, establishment in regulatory frameworks and construction of suitable storage locations.[3] In combination with biomass-based energy sources (BECCUS) as a renewable alternative to fossil fuels, even negative carbon footprints can be achieved, supporting the downscale of anthropogenic greenhouse gas emissions.[4−7] For that, second-generation biomass feedstocks can be converted into (bio)char using pyrolysis technologies. The mostly ligno-

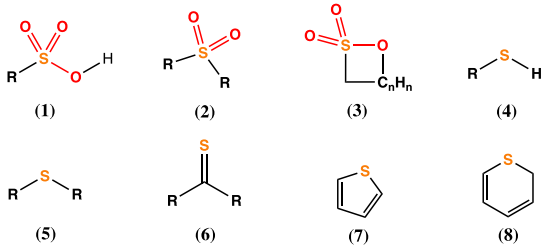



**Figure 1.** Sulfur-containing functional groups (SFGs) in biochars: sulfonic acids (**1**), sulfones (**2**), cyclic sulfonates (**3**), thiols (**4**), thioether (**5**), thioketones (**6**), thiophenes (**7**), and 2*H*-thiopyrans (**8**). **R** exemplifies the organic carbon framework.

**Received:** November 26, 2024
**Revised:** March 18, 2025
**Accepted:** March 19, 2025
**Published:** March 27, 2025



Downloaded via RUHR UNIVERSITAT BOCHUM on April 23, 2025 at 15:43:52 (UTC).
See https://pubs.acs.org/sharingguidelines for options on how to legitimately share published articles.

ACS Publications

© 2025 The Authors. Published by American Chemical Society

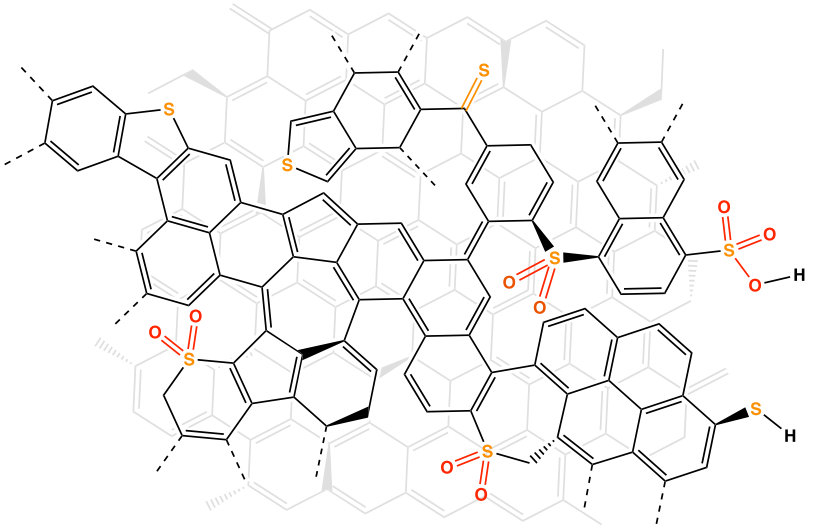


**Figure 2.** Chemical forms of organic sulfur functionalities in a hypothetical (bio)char model system. This char model is constructed from the isolated model systems from Figure 3 implemented in an aromatic hydrocarbon framework.

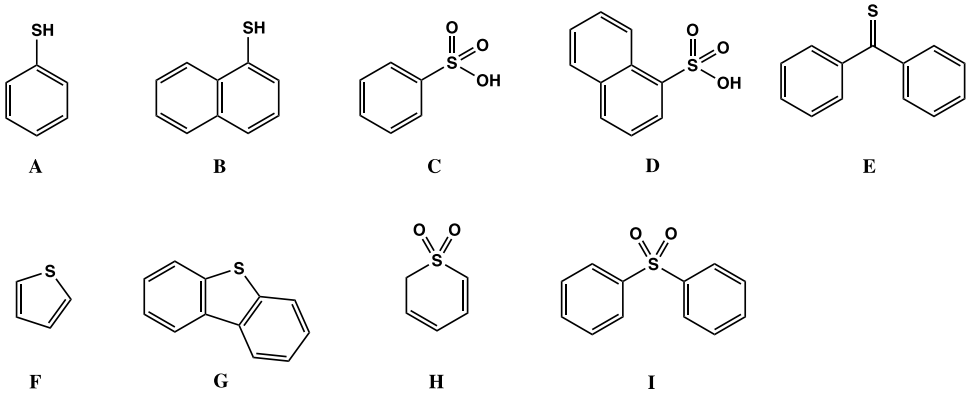



**Figure 3.** Molecular model systems employed in the current work to represent different SFGs: **A**,**B**: thiols, **C**,**D**: sulfonic acids, **E**: thioketones, **F**,**G**: thiophenes, and **H**,**I**: *S*,*S*-dioxides.

cellulosic structure of biomass is converted into a residue of porously stacked graphene-like hydrocarbon layers with several geometric defects and distortions. Nonetheless, it is difficult to chemically characterize char systems due to the nonuniquely defined atom composition, which varies depending on the biomass feedstock, pyrolysis temperature, and pretreatment.[8−11] The carbon framework contains areas of high aromaticity that are doped with several heteroatomic functional groups, mainly comprising oxygen, nitrogen, and sulfur groups.[12−14] In a global perspective, the design of more efficient oxy-fuel burners and process technologies for the combustion of (bio)chars requires more predictive and general computational combustion models than available today. Next to the porosity and surface area, the abundance of heteroatomic functional groups increases the reactivity of the char and can contribute to a faster burnout process compared to unfunctionalized polyaromatic hydrocarbons.[15] Present research on chemical reaction pathways and molecular mechanisms of oxygen functional groups (OFGs) has led to a broad understanding of char burnout and the specific role of OFGs in char combustion on a molecular level.[16−18] While the reaction pathways and mechanisms of OFGs during char burnout were partially explored by Yönder et al.,[19,20] sulfur functional groups (SFGs) have received only limited attention in the literature and have rarely been studied in the context of solid fuel combustion.[21−23] Besides oxygen and nitrogen, sulfur is one of the most abundant heterocomponents in chars. Hence, gaining access to predictive models for char burnout processes accounting for $SO_x$ pollutant formation is important for the enhancement of oxy-fuel engineering.[24,25] In this work we investigate the reaction pathways of SFGs in chars on a molecular level and provide free reaction and activation energies and rate constants that are the basis for future microkinetic models of biochar combustion.[26]

Sulfur can exist in (bio)char in its organic (C−S, C = S) and inorganic forms (sulfates, sulfites).[21] Previous studies investigated the occurrence of organic sulfur in char systems with theoretical and experimental techniques determining the main abundant sulfur functionalities to be thiophenes, sulfonic acids, thiols, thioketones, and cyclic *S*,*S*-dioxides.[14,21,27,28] In general, next to inorganic and elemental sulfur, the covalently bonded SFGs can be differentiated into three types: (i) aromatic/embedded, (ii) C−S bonded sulfur derivatives, and (iii) sulfonic acids.[21] Figure 1 schematically depicts common SFGs in (bio)chars. While sulfonic acids, thioketones and thiols are classified as terminal functionalities, sulfur-containing heterocycles, sulfonates and organic sulfides (thioethers) are considered as embedded SFGs. Conversely, among the SFGs, thiophenic heterocycles are one of the major species formed



https://doi.org/10.1021/acs.jpca.4c07973
J. Phys. Chem. A 2025, 129, 3300−3314

during the pyrolytic conversion of biomass,[21,27] which was experimentally validated by Chen et al.[29] applying XPS and XAS spectroscopy to rhodophytic biochar feedstocks. Figure 2 illustrates a hypothetical molecular cutout of a carbon framework including the main abundant SFGs found in chars. Besides, due to the valency of sulfur, SFGs are located near or at the edge of char systems.[21,30]

The aim of the current study to model at a qualitative level the structural groups and elementary reaction steps involved in the combustion of char-derived systems as to provide the input that is necessary to further refine combustion models as e.g. that proposed in ref 31. For this we employ the model compounds shown in Figure 3 that have been constructed by implementing the SFGs from Figure 1 in benzene- and naphthalene-sized systems that allow to use correlated electronic structure methods beyond density functional theory that are needed to obtain qualitatively correct thermodynamic and kinetic results. Specifically, the current work extends the scope of previous work[19,32] toward the SFGs and the investigation of how these groups evolve in the initial oxidation steps, excluding the oxidation reactions of the carbon backbone. Furthermore, it is determined how the molecular mechanisms change with increasing system sizes, allowing us to extrapolate the reactive behavior of SFGs to larger and more complex (bio)char systems. We apply molecular dynamics (MD) simulations with the reactive force field ReaxFF[33] to explore the reaction space and analyze different reaction channels in the initial combustion phase. The MD trajectories were analyzed by an automatized workflow developed by Schmitz et al.,[34] scanning for reactive events that are refined with higher-level electronic structure calculations. Next to molecular reaction mechanisms, we report reaction energies, activation barriers, and also rate constants as a function of temperature, where we aim at qualitative trends for the combustion of different functional groups in heterogeneous solid fuels rather than quantitative accuracy for a specific compound.

## METHODS

**Molecular Dynamics Simulations.** All molecular dynamics (MD) simulations were carried out using our in-house Python interface pylmps[35] to the MD simulation program LAMMPS.[36] It includes a reimplementation of the reactive force field ReaxFF[33] with the HCONSB parametrization optimized for the combustion branch.[37] The oxidation process of each model system from Figure 3 was simulated within the canonical ensemble and periodic boundary conditions. The cubic simulation box with a volume of 64 $nm^3$ contains 40 $O_2$ molecules and 10 hydroxyl radicals (HO·). Hydroxyl radicals were added to the combustion atmosphere due to their abundance and important role in fuel oxidation[38−40] and to speed up the char burnout process itself. For each system, five MD runs were carried out with different randomly chosen velocity vectors. Each run was started with a heat-up stage of 50 fs and a time step of $\tau = 0.1$ fs and ran 500 ps at 2000 K applying the Nosé-Hoover thermostat.

**Quantum Chemical Calculations.** The analysis of the trajectory followed by a quantum chemical refinement was realized by applying the automated workflow described in detail in ref 34. We laid the focus on the initial combustion reactions of the SFG systems shown in Figure 3 and analyzed their reaction behavior only until sulfur was eliminated from the organic carbon framework as gas-phase species. All QM calculations were carried out using the TURBOMOLE program package[41] (version 7.6[42]). Orbital occupations and spin states have been determined by initial DFT calculations with Fermi smearing followed by subsequent spin-unrestricted calculations for a small range of quantum numbers for the $z$ component of the spin as described in more detail in ref 34. In the current study, we found for the majority of structures that the ground-state has either a closed-shell singlet or doublet configuration with a single unpaired electron. For all molecular structures with two unpaired electrons we found triplet ground states. All DFT calculations employed the resolution of identity (RI-J) approximation[43] for the Coulomb potentials with optimized auxiliary basis sets[44] and Grimme's D3 dispersion correction.[45] First, the initial structures and reaction products were optimized using DFT with the TPSS meta-GGA functional[46] and the def-SVP basis set.[47] The final geometries and electronic energies were obtained using the TPSSh meta-hybrid exchange-correlation functional[48] and the TZVP basis set.[49] For these calculations we employed the `ridft` and `rdgrad` programs of the TURBOMOLE package. The scaled zero-point vibrational (ZPV) energy (using the scaling factor 0.9874 for the TPSSh functional from ref 50) was added to the electronic energy. Electronic reaction $E_{rxn}$ and activation energies $E_{act}$ were calculated via eqs 1 and 2, respectively. Here, $E_{ZPV,i}$ is defined as the ZPV energy of molecular species $i$ with an electronic energy $E_{el,i}$. The electronic energy of the transition state for a given reaction is denoted with $E_{el,TS}$.

$$E_{rxn} = \sum_{i}^{products} (E_{el,i} + E_{ZPV,i}) - \sum_{i}^{reactants} (E_{el,i} + E_{ZPV,i}) \quad (1)$$

$$E_{act} = E_{el,TS} + E_{ZPV,TS} - \sum_{i}^{reactants} (E_{el,i} + E_{ZPV,i}) \quad (2)$$

For the calculation of temperature-dependent reaction rate constants, the electronic energies were further refined with the `ccsdf12` module using explicitly correlated coupled cluster singles and doubles with a perturbative correction for connected triples, CCSD(F12*)(T*).[51] All CC calculations use the frozen-core approximation applied to the $1s^2$ core of carbon and oxygen and the $1s^22s^22p^6$ core sulfur and the cc-pVDZ-F12 orbital,[52] auxiliary,[53,54] and complementary auxiliary basis sets[55] in combination with the recommended exponent[52] of 0.9 for the correlation factor in the F12 geminals. Restricted open-shell Hartree−Fock (ROHF) for open-shell and usually restricted Hartree−Fock calculations for closed-shell systems were done with the `dscf` module[56] and used as the reference wave function for the CC calculations. The difference the CCSD-(F12*)[T] and CCSD(F12*)(T) results was used to check for possible multireference situations where single-reference methods and in particular the perturbative triples correction would fail. This difference is for systems reported in the following below 32.3 kJ/mol, which we judge to be sufficient for the qualitative accuracy we are aiming at.

Reaction pathways were determined with the chain-of-state method[57−59] implemented in the `woelfling` program, and transition states optimized with the trust-region image minimization algorithm[60] (module `statpt`) and validated by intrinsic reaction coordinate calculations (module `DRC`). Reaction rate constants $k$ of reactions with a significant activation barrier were calculated using transition state theory with the ideal gas law as the equation of state at a constant pressure of $P = 1$ bar (eq 3).[32]



https://doi.org/10.1021/acs.jpca.4c07973
J. Phys. Chem. A 2025, 129, 3300−3314

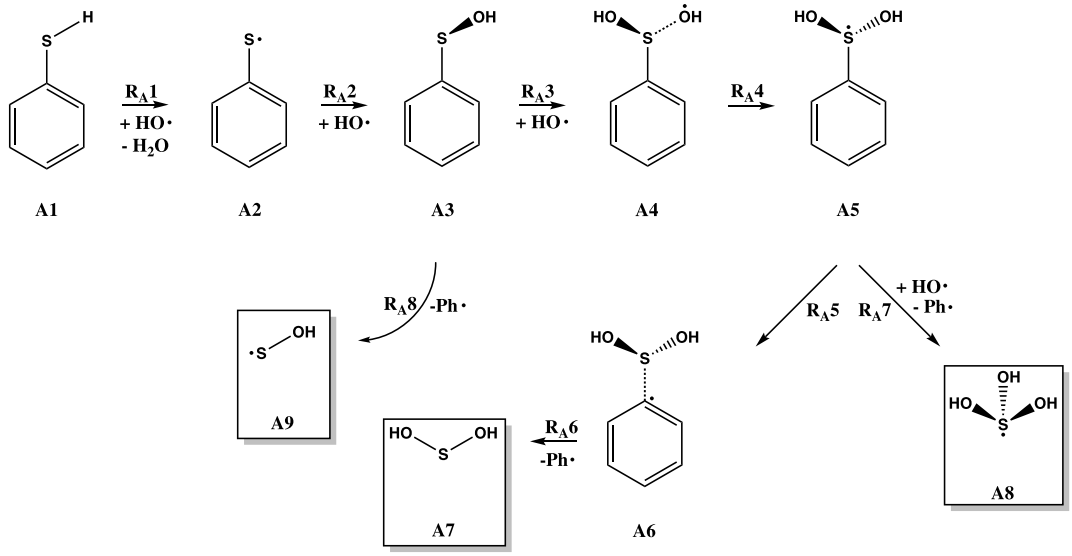



**Figure 4.** Oxidation pathways for thiophenol (**A**).

$$k(T) = \kappa \frac{k_b T}{h} \frac{Q_{TS}/V}{\Pi_{i=\text{educts}}(Q_i/V)} \exp\left(-\frac{E_{el,act}}{RT}\right) \quad (3)$$

Here $Q_{TS}$ denotes the partition function of the transition state and $Q_i$ the one of a given species that are obtained by applying a modified rigid rotor harmonic oscillator approximation (qRRHO).[32,61] Furthermore, $R$ is the ideal gas constant, $T$ the absolute temperature, $V$ the molar volume, $h$ the Planck constant, $k_b$ the Boltzmann constant, and $E_{el,act}$ the electronic activation energy for the transition state. The transmission coefficient $\kappa$ is computed within the high-temperature limit of the Eckart tunneling correction, which asymptotically approaches the Wigner tunneling correction (eq 4).[62] Let $\nu$ be the imaginary frequency of the transition state, then $\kappa$ is given within this approximation as

$$\kappa = 1 - \frac{1}{24}\left(\frac{h\nu}{k_b T}\right)^2 \left(1 + \frac{RT}{E_{el,act}}\right) \quad (4)$$

With eq 3 temperature-dependent reaction rate constants were calculated on a grid for the temperature range of 300 to 3000 K. To interpolate between the computed points, the results are fitted to a modified Arrhenius equation,

$$k = AT^n \exp\left(-\frac{E}{T}\right) \quad (5)$$

via the parameters $A$, $n$, and $E$, to provide qualitative kinetic data for the reactions at sulfur containing functional groups in a format that is widely used in combustion modeling.[63,64]

## RESULTS AND DISCUSSION

**Thiols.** Thiols contain sulfhydryl groups (−SH) representing the sulfur analogues of alcohols.[65] Previous research on thiophenol typically only considered sulfur elimination pathways and S-migration reactions during pyrolysis conditions combining experimental and theoretical data.[66,67] For the initial reaction steps of pyrolysis, it has been reported that thiophenol can react to thioketones or is dehydrogenated and the main abundant elimination products are yet missing in the literature. We studied them here at the example of the two smallest but most important aromatic thiols: thiophenol and thionaphthol.

**Table 1. TPSSh-D3/TZVP and CCSD(F12*)(T*)/cc-pVDZ-F12 Energies for Oxidation Pathways of Compound A in kJ/mol**

| reaction | $E_{act,DFT}$ | $E_{rxn,DFT}$ | $E_{act,CC}$ | $E_{rxn,CC}$ |
|---|---|---|---|---|
| A1 + HO· → A2 + $H_2O$ | barrierless | −145.6 | | −155.7 |
| A2 + HO· → A3 | barrierless | −233.1 | | −270.8 |
| A3 + HO· → A4 | barrierless | −74.1 | | −50.6 |
| A4 → A5 | 26.5 | 2.5 | 25.7 | −18.3 |
| A5 → A6 | 97.3 | 90.0 | (86.8) | 90.8 |
| A6 → A7 + Ph· | barrierless | 27.0 | | 16.3 |
| A5 + HO· → A8 + Ph· | 95.1 | 34.0 | 74.7 | 14.8 |
| A3 → A9 + Ph· | barrierless | 303.8 | | 390.6 |
| A1 + HO· → A10 | barrierless | −69.6 | | −74.6 |
| A1 + HO· → A11 + $H_2O$ | barrierless | −6.4 | | −22.1 |
| A1 + HO· → A12 + $H_2O$ | barrierless | −10.7 | | −25.3 |
| A1 + HO· → A13 + $H_2O$ | barrierless | −9.9 | | −24.1 |

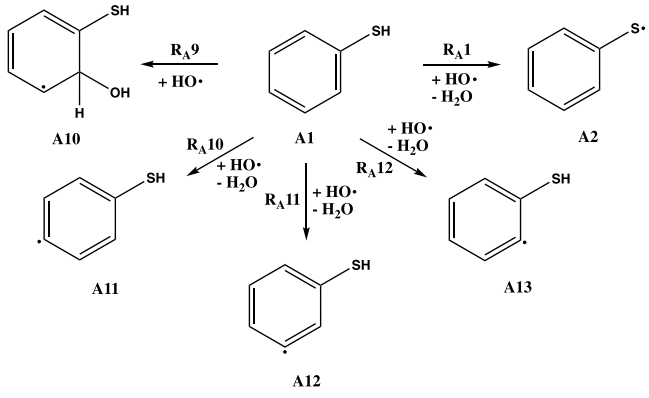



**Figure 5.** Comparison of the H abstraction from the −SH group with alternative initial reaction steps for thiophenol (**A**).

In contrast to pyrolysis, oxy-fuel combustion is set up in an oxygen atmosphere leading to different elimination and reaction products than observed for pyrolysis.[66,67] Li et al. investigated a large-scale molecular lignite system that contained thiols, thiophenes, and thioether using ReaxFF and DFT methods.[68] However, detailed mechanistic insights addressing the initial


https://doi.org/10.1021/acs.jpca.4c07973
J. Phys. Chem. A 2025, 129, 3300−3314

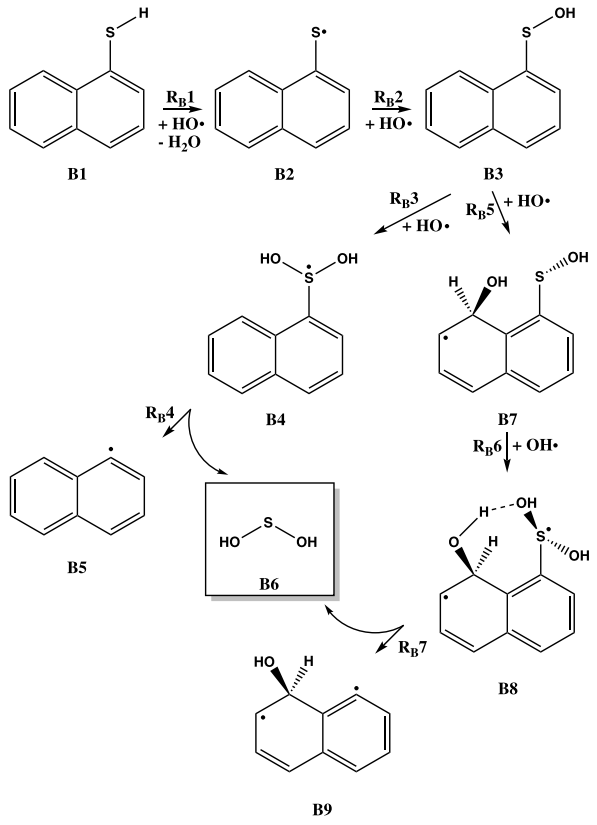



**Figure 6.** Oxidation pathways for naphthalene-1-thiol (**B**).

**Table 2. TPSSh-D3/TZVP and CCSD(F12*)(T*)/cc-pVDZ-F12 Energies for Oxidation Pathways of Compound B in kJ/mol**

| reaction | $E_{act,DFT}$ | $E_{rxn,DFT}$ | $E_{act,CC}$ | $E_{rxn,CC}$ |
|---|---|---|---|---|
| B1 + HO· → B2 + $H_2O$ | barrierless | −157.0 | | −162.4 |
| B2 + HO· → B3 | barrierless | −223.4 | | −265.0 |
| B3 + HO· → B4 | barrierless | −37.2 | | −50.0 |
| B4 → B5 + B6 | barrierless | 83.8 | | 91.0 |
| B3 + HO· → B7 | barrierless | −96.6 | | −96.5 |
| B7 + HO· → B8 | barrierless | −84.0 | | −76.4 |
| B8 → B6 + B9 | barrierless | 127.4 | | 113.4 |

oxidation reactions through channels involving gas-phase radical species are missing.

*Thiophenol.* In thiophenol, the initial oxidation steps lead to the formation of $SO_xH_x$ oxides (Figure 4). Hydroxyl radicals (HO·) react directly with thiol functionalities forming thiyl radicals (**A2**), that can recombine with HO· to benzene sulfenic acid **A3** (phenyl sulfanol). At this point, three oxidation pathways were examined leading to the species **A7**, **A8**, and **A9**.

Terminal thiol groups undergo stepwise oxidation by hydroxyl radicals contained in the combustion atmosphere. It was found for system **A** that in all MD runs the initial oxidation steps are initiated by HO· radicals and occur at the terminal S-functionality. Sulfur is eliminated as $SO_xH_x$ ($x$ = 1,2,3) from the aromatic system before the carbon framework is oxidized. The three elimination products (**A7**, **A8** and **A9**) can convert into each other or are further oxidized in the radical-rich combustion atmosphere. Either HOS· is directly eliminated or species **A3** forms a noncovalently bound complex (**A4**) with an additional HO· radical prior to forming the intermediate structure **A5**. As

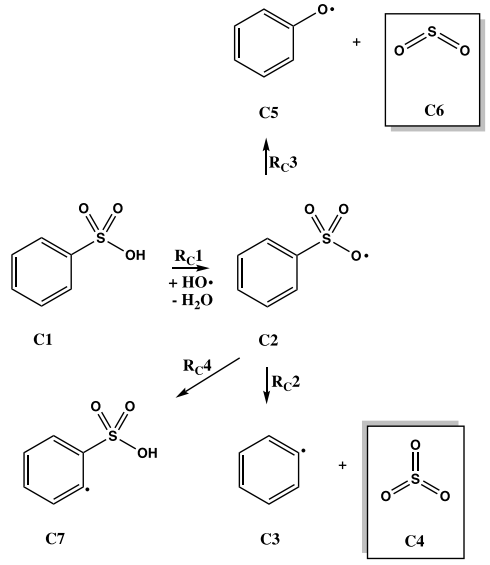



**Figure 7.** Oxidation pathways for benzene sulfoxylic acid (**C**).

**Table 3. TPSSh-D3/TZVP and CCSD(F12*)(T*)/cc-pVDZ-F12 Energies for Oxidation Pathways of Compound C in kJ/mol**

| reaction | $E_{act,DFT}$ | $E_{rxn,DFT}$ | $E_{act,CC}$ | $E_{rxn,CC}$ |
|---|---|---|---|---|
| C1 + HO· → C2 + $H_2O$ | barrierless | −62.7 | | −30.3 |
| C2 → C3 + C4 | barrierless | 128.1 | | 102.2 |
| C2 → C5 + C6 | 63.2 | −107.8 | 55.3 | −78.6 |
| C2 → C7 | 116.8 | 51.5 | 107.2 | 13.7 |

can be seen in Table 1, the electronic energies indicate that the elimination of **A7** and **A8** is thermodynamically favored compared to the elimination of the HOS· species. The decomposition of **A3** into a HOS· radical ($R_A8$) needs 390.6 kJ/mol of energy and is therefore thermodynamically disfavored. Much more important is the reaction channel $R_A3$ (Table 1). While the reaction energy for the $H_3O_3S$· elimination is 14.8 kJ/mol with an activation energy of 74.7 kJ/mol, the elimination of $SO_2H_2$ has no significant activation barrier. For the endothermic reaction $R_A5$ we find on the DFT potential energy surface a small barrier of 7.3 kJ/mol for the backward reaction which seems to not exist on the CC potential energy surface as we find in the CC calculation for the DFT-optimized transition state structure an energy below that of **A6**.

As pointed out in the introduction, the focus of the current study is on oxidation reaction channels initiated at sulfur functional groups. To provide a comparison with reaction channels initiated at other sites, in particular aromatic rings, we investigated for thiophene also reaction channels starting with a reaction at the benzene ring (Figure 5). Hydroxyl radicals can abstract hydrogen atoms from aromatic rings without a barrier. These reactions lead for thiophene to the open-shell compounds **A11**−**A13** and is in all cases nearly 130 kJ/mol less exothermic compared to the abstraction of a hydrogen atom from the thiol group (Figure 1). Another possible reaction channel observed in the MD simulations is the *ortho*-addition of a hydroxyl radical to the benzene ring forming species **A10** with a reaction energy of −74.6 kJ/mol. The much less favorable energetics of these reactions emphasize that oxidation reactions at SFGs are important initiation steps for the combustion of sulfur-containing (bio)char.


https://doi.org/10.1021/acs.jpca.4c07973
J. Phys. Chem. A 2025, 129, 3300−3314

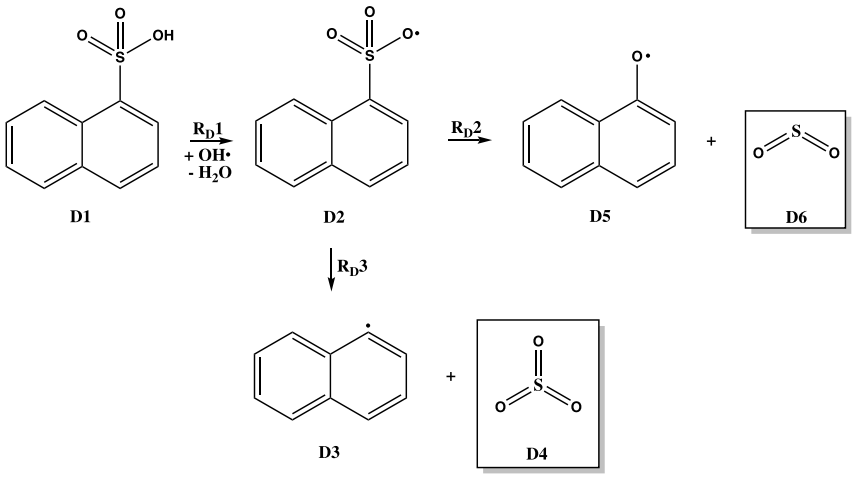



**Figure 8.** Oxidation pathways for naphthalene-1-sulfonic acid (**D**).

**Table 4. TPSSh-D3/TZVP and CCSD(F12*)(T*)/cc-pVDZ-F12 Energies for Oxidation Pathways of Compound D in kJ/mol**

| reaction | $E_{act,DFT}$ | $E_{rxn,DFT}$ | $E_{act,CC}$ | $E_{rxn,CC}$ |
|---|---|---|---|---|
| D1 + HO· → D2 + $H_2O$ | barrierless | −70.7 | | −33.1 |
| D2 → D3 + D4 | barrierless | 135.9 | | 96.2 |
| D2 → D5 + D6 | 48.0 | −128.8 | 20.8 | −112.1 |

*Naphthalene-1-thiol.* Next, we investigated the oxidation pathways of naphthalene-1-thiol to study how much the oxidation pathways of aromatic thiols change with the system size. The results (compare Figure 6) show that the oxidation mechanisms are similar to the ones observed in system **A**. In the initial reaction steps, the thiol group is dehydrogenated ($\mathbf{R_B1}$) before to the thiyl-radical reacts with two hydroxyl radicals forming sulfoxylic acid ($SO_2H_2$). This reaction was found to occur either before the carbon structure is attacked by hydroxyl radicals or at a partially oxidized carbon framework. In the first case, the open-shell thiyl radical species **B2** recombines with one hydroxyl radical ($\mathbf{R_B2}$) forming a sulfenic acid derivative **B3** that is similar to species **A3**. Also, the reaction energies (Table 2) are consistent, being 5.8 kJ/mol higher for naphthalene-1-thiol compared to thiophenol. At this reaction step, it was discovered that **B3** can react directly to a sulfur hydroxide group (**B4**) before eliminating sulfoxylic acid (**B6**). As for thiophenol, the elimination of $SO_2H_2$ has no significant barrier and a reaction energy of 91 kJ/mol (0.2 kJ/mol higher than for thiophenol). Beyond that, it was also discovered that the carbon structure itself can be attacked by one hydroxyl radical forming the partially oxidized sulfenic acid species **B7**. Next, the sulfenic group is further oxidized ($\mathbf{R_B7}$) similar to reaction $\mathbf{R_B3}$ eliminating again sulfoxylic acid which requires an energy of 113.4 kJ/mol. In all MD runs of the naphthalene-1-thiol system, sulfur is eliminated as $SO_2H_2$ from the carbon backbone.

**Sulfonic Acids.** Recent studies that investigated sulfur oxo-acid reaction pathways are limited to biologically important sulfenic acids[69] and small oxo S-species.[70] While Zaman investigated the pyrolysis of $C_6$-based sulfonic acids at a macroscopic level,[71] detailed mechanistic studies of the oxidation pathways of benzene- and naphthalene-sized sulfonic acids are lacking in the literature.

*Benzenesulfonic Acid.* The combustion of benzenesulfonic acid (Figure 7) starts with the abstraction of a hydrogen atom from the acid form (**C1**) by an HO· radical forming a $-SO_3$· radical group (**C2**). In the ReaxFF simulations, two subsequent pathways to $SO_x$ volatiles were observed for **C2**. One reaction channel ($\mathbf{R_C2}$) leads to the dissociation of the C−S bond and the formation of a phenyl radical (**C3**) and sulfur trioxide (**C4**). Alternatively, **C2** can react ($\mathbf{R_C3}$) to a phenoxyl radical (**C5**) and sulfur dioxide (**C6**). **C2** can rearrange to its acid form (**C7**) by shifting a hydrogen atom from the phenyl ring to one of the oxygen atoms in the $-SO_3$· group. While the elimination of $SO_3$ is endothermic (102.2 kJ/mol) the reaction to $SO_2$ is exothermic with an activation energy of 55.3 kJ/mol and is thus energetically favored (Table 3).

Zaman[71] studied the pyrolysis of benzene systems containing sulfonic acid functionalities and reported that sulfur dioxide is the main sulfur oxide compound formed during the conversion process. In the current study we find that also for the oxidation of sulfonic acids the elimination of of sulfur dioxide is an important reaction channel. In contrast to other terminal SFGs, the sulfonate group is already maximally oxidized as a C−S bonded group. Hence, the elimination of $SO_2$ and $SO_3$ is observed in the ReaxFF simulations, and as seen for the thiol and thioketone systems, the initial oxidation mechanism starts with the dehydrogenation of the acid group by HO· radicals, forming eventually $SO_x$ species.

Sulfur dioxide and other sulfur oxide volatiles react with atomic and molecular oxygen or hydroxyl radicals to higher oxidized $SO_xH_y$ intermediates in the oxy-fuel atmosphere. As we focus in the current study on the initial oxidation and elimination pathways of SFGs in aromatic hydrocarbons we refer for the combustion reactions of $SO_2$ and $SO_3$ to the work of Hindiyarti et al.[72] The hydrogen shift reaction leading to **C2**, generates aryl radicals that can initiate additional radical branching reactions[73,74] and thereby open new reaction channels to oxo-radicals that consume molecular oxygen.[19]

*Naphthalene-1-sulfonic Acid.* Also for the larger naphthalene sulfonic acid **D1** the sulfonic acid group eliminates as sulfur dioxide or sulfur trioxide (Figure 8), similar as in its benzene counterpart. In system **D**, the $SO_3$ elimination is with a reaction energy of 96.2 kJ/mol less endothermic compared to the benzene-sized sulfonic acid (Table 4). Interestingly, the activation energy of the $SO_2$ elimination pathway is 34.5 kJ/mol lower compared to the same reaction in system **C**. Overall, system **C** and **D** show a similar reactive behavior during the initial oxidation steps of the $-SO_3H$ group. In both systems, the


https://doi.org/10.1021/acs.jpca.4c07973
J. Phys. Chem. A 2025, 129, 3300−3314

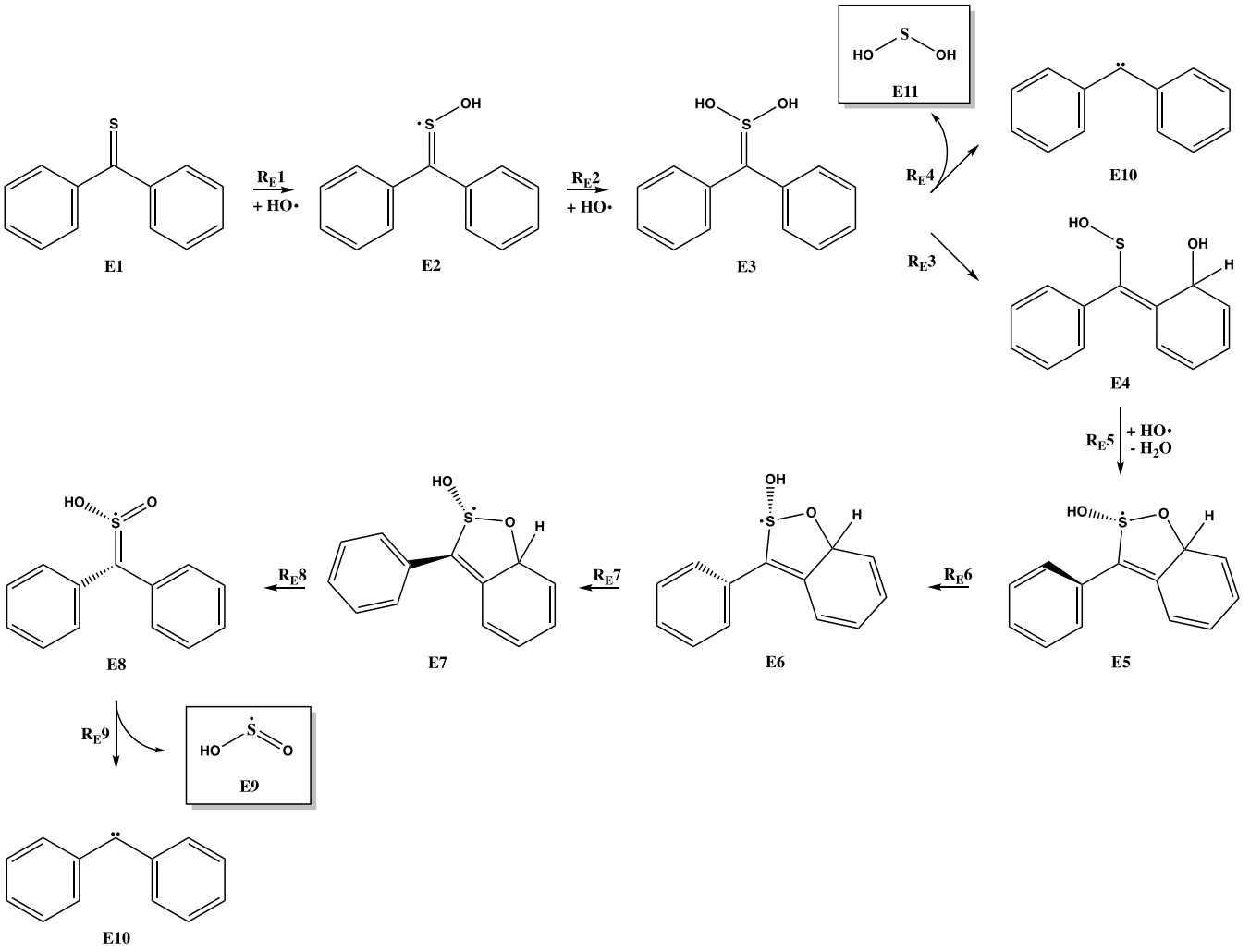



**Figure 9.** Oxidation pathways for diphenylmethanethione (**E**).

**Table 5. TPSSh-D3/TZVP and CCSD(F12*)(T*)/cc-pVDZ-F12 Energies for Oxidation Pathways of Compound E in kJ/mol**

| reaction | $E_{act,DFT}$ | $E_{rxn,DFT}$ | $E_{act,CC}$ | $E_{rxn,CC}$ |
|---|---|---|---|---|
| E1 + HO· → E2 | barrierless | −124.7 | | −133.9 |
| E2 + HO· → E3 | barrierless | −103.9 | | −121.9 |
| E3 → E4 | barrierless | −75.9 | | −87.0 |
| E3 → E10 + E11 | barrierless | 169.1 | | 161.6 |
| E4 + HO· → E5 + $H_2O$ | barrierless | −99.4 | | −96.3 |
| E5 → E6 | 74.4 | 55.8 | 51.8 | 25.6 |
| E6 → E7 | 5.4 | −13.4 | 0.8 | −11.0 |
| E7 → E8 | 5.9 | −133.3 | 0.9 | −163.6 |
| E8 → E9 + E10 | barrierless | 225.2 | | 250.2 |

reaction to sulfur dioxide is the energetically favored reaction pathway, which was also observed experimentally by Zaman.[71]

**Thioketones.** As an example for thiocarbonyl functionalities, we investigated the oxidation pathways (Figure 9) of diphenylmethanethione. This compound shows a reaction behavior comparable to other terminal SFGs, namely the stepwise oxidation of the sulfur atom to sulfoxylic acids. In the first (barrierless) reaction step, a hydroxyl radical adds to the thioketone functionality, forming the open-shell sulfenic acid **E2**. The addition of a second hydroxyl radical leads without significant barrier to the intermediate sulfanediol **E3** with a reaction energy of −121.9 kJ/mol (Table 5). Starting from **E3**, two potential reaction pathways were observed: the elimination of sulfoxylic acid ($\mathbf{R_E4}$) and the formation of an open-shell oxathiolane derivative ($\mathbf{R_E3}$). The direct elimination of $SO_2H_2$ forming diphenylmethylene (**E11**) requires 161.6 kJ/mol of energy. In contrast to this endothermic reaction, the pathway to species **E4** and **E5** proceeds via two exothermic steps, releasing −87.0 kJ/mol ($\mathbf{R_E3}$) and −96.3 kJ/mol ($\mathbf{R_E4}$), respectively. After some rotational rearrangements ($\mathbf{R_E6}$–$\mathbf{R_E8}$), eventually $HO_2S$· is eliminated, forming **E10** in a highly endothermic reaction that requires 250.2 kJ/mol.

**Thiophenes.** Previous studies on combustion reactions of thiophenes focused on the mechanisms and kinetics of thiophene reacting with hydroxyl radicals[75−77] and pyrolysis reactions.[78,79] More detailed studies were carried out analyzing unimolecular pyrolysis mechanisms of larger aromatic thiophene systems such as benzothiophene and dibenzothiophene.[80−82] However, at present, theoretical studies of oxidation mechanisms of thiophenes in an oxygen atmosphere, including activation energies and kinetic parameters, are limited.

*Thiophene.* The initial steps for the oxidation of thiophene (**F1**) are summarized in Figure 10. In the first reaction step ($\mathbf{R_F1}$), a hydroxyl radical adds to the $\alpha$-carbon atom, forming the 2-hydroxyl open-shell system **F2** in a barrierless reaction (Table


https://doi.org/10.1021/acs.jpca.4c07973
J. Phys. Chem. A 2025, 129, 3300−3314

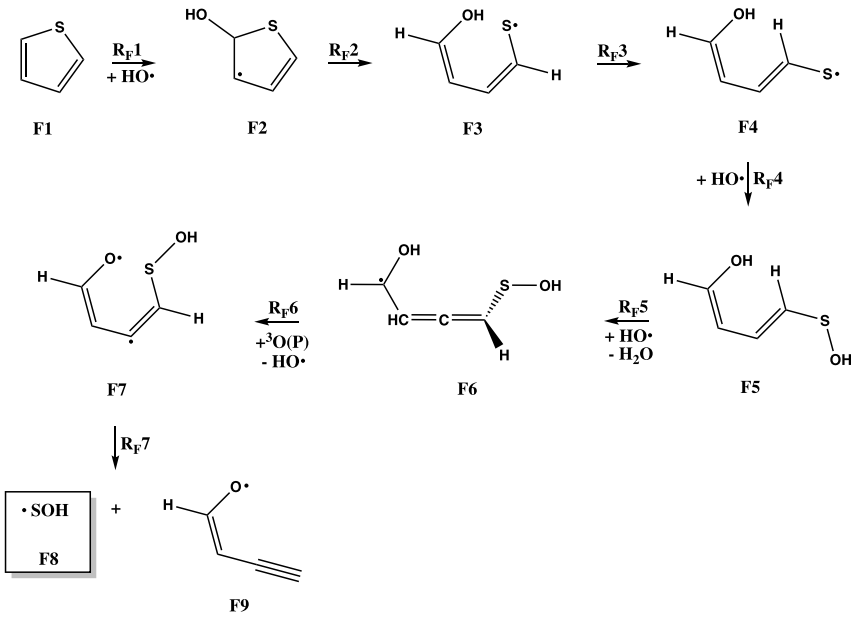



**Figure 10.** Oxidation pathways for thiophene (**F**).

**Table 6. TPSSh-D3/TZVP and CCSD(F12*)(T*)/cc-pVDZ-F12 Energies for Oxidation Pathways of Compound F in kJ/mol**

| reaction | $E_{act,DFT}$ | $E_{rxn,DFT}$ | $E_{act,CC}$ | $E_{rxn,CC}$ |
|---|---|---|---|---|
| F1 + HO· → F2 | barrierless | −116.6 | | −102.9 |
| F2 → F3 | 76.8 | 37.6 | 100.5 | 58.3 |
| F3 → F4 | 48.0 | −27.8 | 34.9 | −25.9 |
| F4 + HO· → F5 | barrierless | −205.0 | | −252.0 |
| F5 + HO· → F6 + $H_2O$ | barrierless | −70.8 | | −76.5 |
| F6 + $^3O(P)$ → F7 + HO· | barrierless | −116.2 | | −104.1 |
| F7 → F8 + F9 | 80.3 | 74.9 | 89.8 | 71.1 |

6). In the next step, the C−S bond breaks homolytically, forming **F3**. Subsequent to a rotational rearrangement ($R_F3$) a second hydroxyl radical adds, forming the sulfenic acid derivative **F5**. After two dehydrogenation reactions ($R_F5$, $R_F6$) the open-shell HOS· radical **F8** is eliminated, yielding the hydrocarbon species **F9**. The HOS· elimination has an activation energy of 89.8 kJ/mol and is endothermic, requiring 71.1 kJ/mol of energy.

*Dibenzo[b,d]thiophene.* The oxidation of dibenzothiophene (Figure 11) is initiated by the formation of an aryl radical in one of the benzene rings (**G2**) which can rearrange to a five- and a three-membered ring (**G3**). In the latter intermediate, the *β*-*γ* C−C bond dissociates homolytically, leading to a vinyl-radical

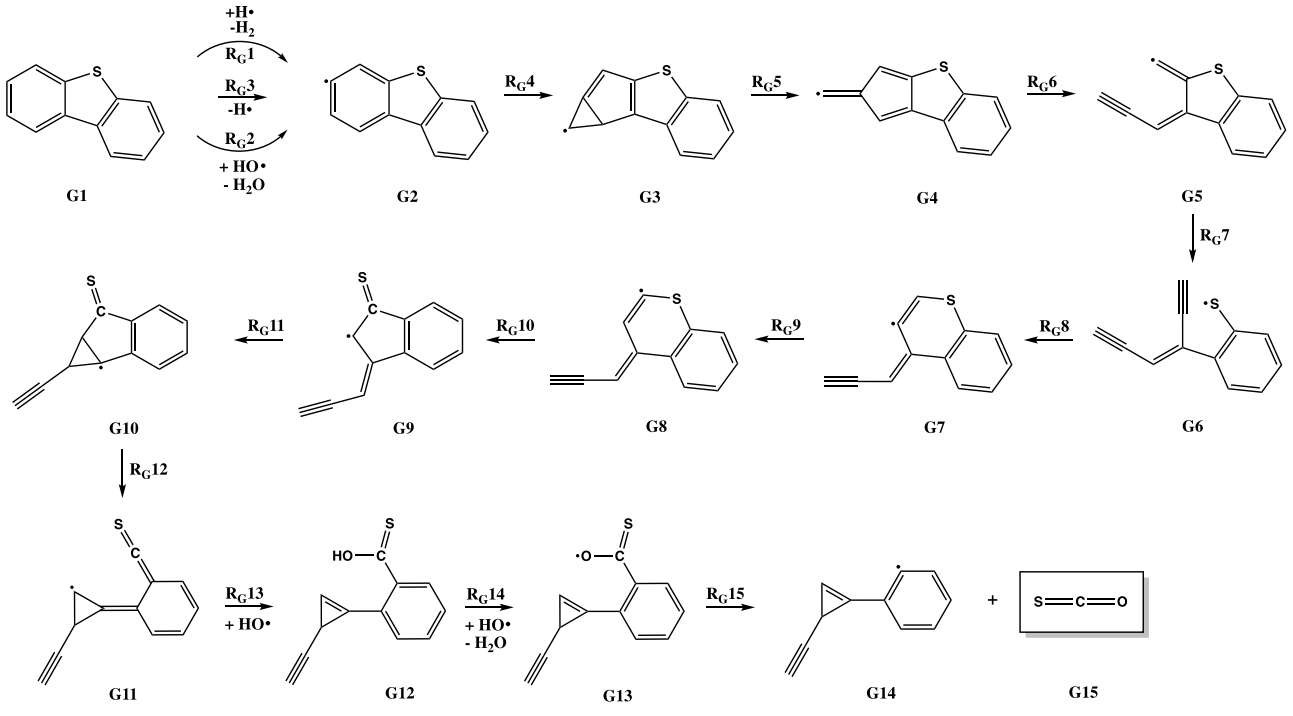



**Figure 11.** Oxidation pathways for dibenzo[b,d]thiophene (**G**).



https://doi.org/10.1021/acs.jpca.4c07973
J. Phys. Chem. A 2025, 129, 3300−3314

**Table 7. TPSSh-D3/TZVP and CCSD(F12*)(T*)/cc-pVDZ-F12 Energies for Oxidation Pathways of Compound G in kJ/mol**

| reaction | $E_{act,DFT}$ | $E_{rxn,DFT}$ | $E_{act,CC}$ | $E_{rxn,CC}$ |
|---|---|---|---|---|
| G1 + H· → G2 + $H_2$ | 29.0 | 14.1 | 65.6 | 36.0 |
| G1 + HO· → G2 + $H_2O$ | barrierless | −8.4 | 17.2 | −23.5 |
| G1 → G2 + H· | | 458.7 | | 466.0 |
| G2 → G3 | 247.3 | 232.3 | 255.1 | 238.5 |
| G3 → G4 | 22.0 | −77.4 | 23.5 | −85.4 |
| G4 → G5 | 140.1 | 128.8 | 145.7 | 129.0 |
| G5 → G6 | 58.0 | 41.8 | 64.3 | 36.7 |
| G6 → G7 | 23.3 | −51.6 | 32.2 | −46.7 |
| G7 → G8 | 204.0 | 3.4 | 204.0 | −2.0 |
| G8 → G9 | 126.5 | −161.2 | 143.8 | −140.9 |
| G9 → G10 | 200.5 | 190.6 | 207.3 | 188.0 |
| G10 → G11 | 150.6 | 95.2 | 164.9 | 95.6 |
| G11 + HO· → G12 | barrierless | −374.1 | | −400.8 |
| G12 + HO· → G13 + $H_2O$ | barrierless | −144.3 | | −143.5 |
| G13 → G14 + G15 | barrierless | 75.5 | | 71.4 |

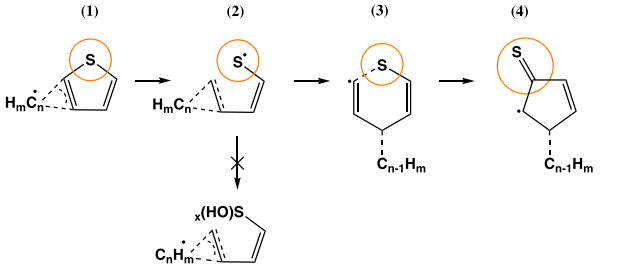



**Figure 12.** Schematic summary of the rearrangements of **G** to thiophenic sulfur (**1**), thiolic sulfur (**2**), thiopyrolic sulfur (**3**), and a thioketone (**4**). Addition reactions of hydroxyl radicals to the sulfur atom were not detected in the simulations.

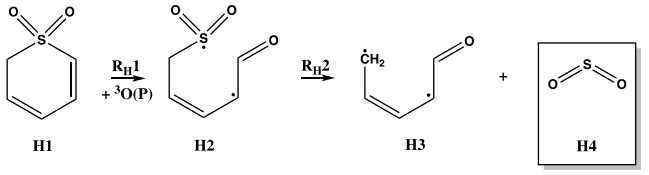



**Figure 13.** Oxidation pathways for thiopyran 1,1-dioxide (**H**).

**Table 8. TPSSh-D3/TZVP and CCSD(F12*)(T*)/cc-pVDZ-F12 Energies for Oxidation Pathways of Compound H in kJ/mol**

| reaction | $E_{act,DFT}$ | $E_{rxn,DFT}$ | $E_{act,CC}$ | $E_{rxn,CC}$ |
|---|---|---|---|---|
| H1 + $^3O(P)$ → H2 | barrierless | −296.0 | | −226.6 |
| H2 → H3 + H4 | barrierless | 52.5 | | 39.1 |

structure **G4**. This exothermic reaction has a relatively low barrier of 23.5 kJ/mol and a reaction energy of −85.4 kJ/mol (Table 7). In reaction $R_G7$ the C−S bond breaks, and the reactive thiyl radical **G6** is formed. The latter rearranges to a thiopyrol derivative, which exists as the two H-tautomers, **G7** and **G8**. Tautomer **G8** can undergo a ring contraction reaction, forming the thioketone **G9**. The latter reaction is highly exothermic (−140.9 kJ/mol) with an activation barrier of 143.8 kJ/mol.

No direct oxidation reactions of the thiyl functionality (−S·) were detected in system **G**, as it has been the case for the

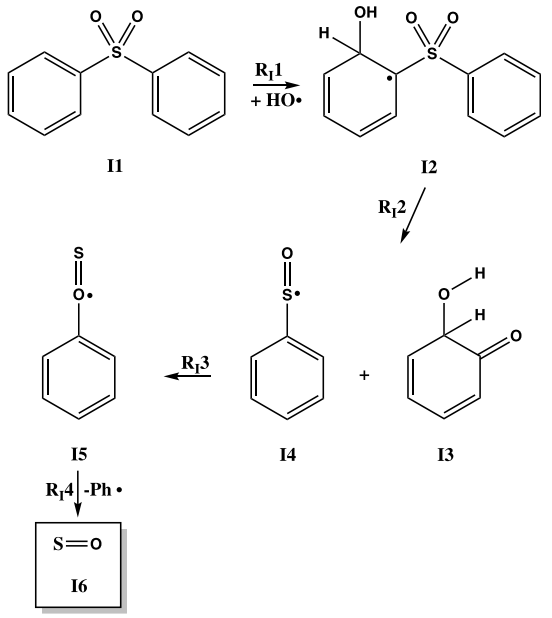



**Figure 14.** Oxidation pathways for sulfonyldibenzene (**I**).

**Table 9. TPSSh-D3/TZVP and CCSD(F12*)(T*)/cc-pVDZ-F12 Energies for Oxidation Pathways of Compound I in kJ/mol**

| reaction | $E_{act,DFT}$ | $E_{rxn,DFT}$ | $E_{act,CC}$ | $E_{rxn,CC}$ |
|---|---|---|---|---|
| I1 + HO· → I2 | barrierless | −73.4 | | −73.2 |
| I2 → I3 + I4 | 211.8 | −91.4 | 266.7 | 14.8 |
| I4 → I5 | 192.5 | 44.9 | 223.0 | 77.2 |
| I5 → I6 + Ph· | barrierless | 208.9 | | 202.4 |

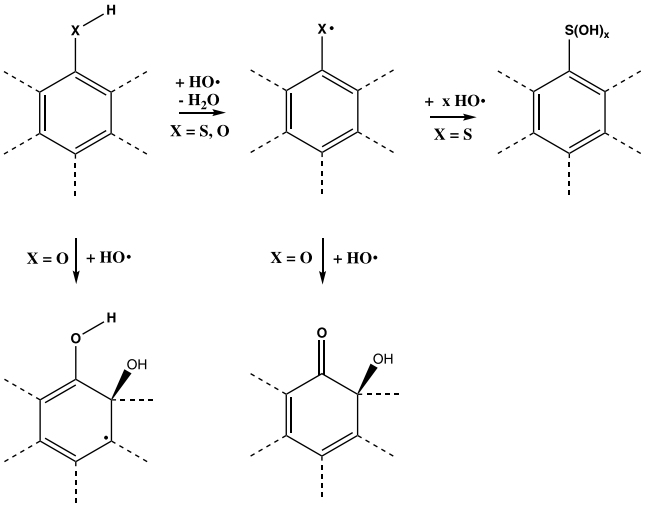



**Figure 15.** Initial reaction steps of thiophenol (X = S) observed in the present study and in phenol (X = O) by Yönder et al.[19]

aromatic thiols **A** and **B** where this led to the formation of $SO_xH_x$ volatiles. Apparently, the intramolecular ring contraction reactions are faster then the reaction of the thiyl radical with HO·.

The thioketone intermediate **G9** converts into a thioketene group in a reaction requiring an activation energy of 164.9 kJ/mol. For an alternative pathway of thioketone functional groups, the reader is redirected to the elimination reactions of system **E**. For compound **G** it was observed that thioketones can form


https://doi.org/10.1021/acs.jpca.4c07973
J. Phys. Chem. A 2025, 129, 3300−3314

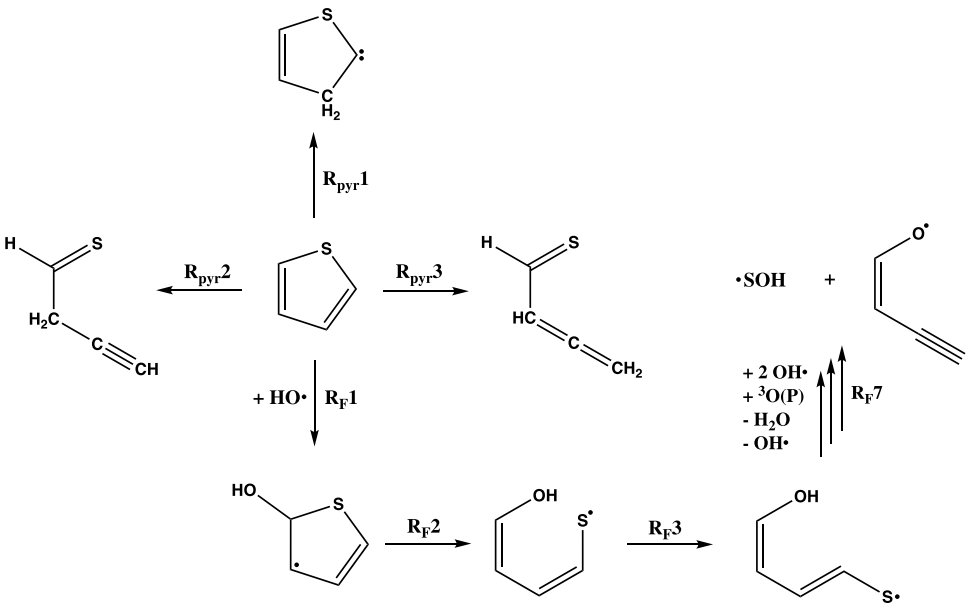



**Figure 16.** Initial pyrolysis reactions of thiophene $\mathbf{R_{pyr}1}$−$\mathbf{R_{pyr}3}$ found by Li et al.[84] compared to the initial reaction channels $\mathbf{R_F1}$−$\mathbf{R_F7}$ for the oxidation of thiophene in an oxy-fuel atmosphere from the present work.

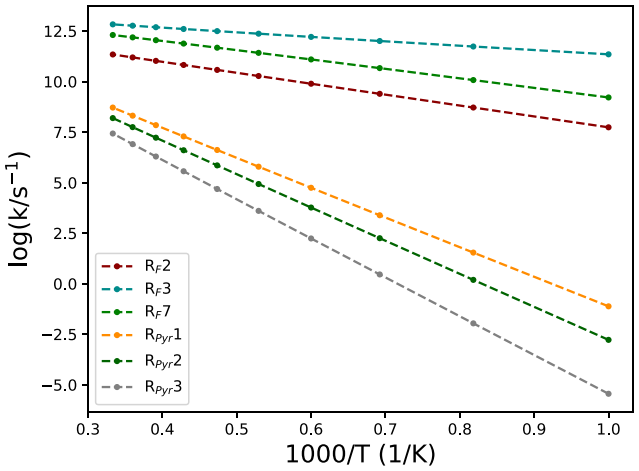



**Figure 17.** Comparison of the rate constants of the thiophene oxidation pathway shown in Figure 10 with the rate constants for the pyrolysis reactions found by Li et al.,[84] recomputed in the current work at the same level of theory as used for the oxidation reactions.

thioketenes before reacting with gas-phase radicals such as HO· ($\mathbf{R_G13}$). This reaction type has no significant barrier and releases −400.8 kJ/mol of energy and yields the carbothioic *O*-acid **G12**. Eventually, after an abstraction of a hydrogen atom from the acid functionality carbonyl sulfide (COS) is eliminated in an endothermic reaction requiring 71.4 kJ/mol of energy.

In contrast to terminal functional groups, thiophenes are embedded into the aromatic system and, hence, the initial reaction steps cannot take place directly at the sulfur atom.[75,83] However, it was found for embedded thiophenic sulfur functionalities that they convert to thiols, thiopyrolic sulfur and, eventually, to thioketones (Figure 12). These reaction pathways of dibenzothiophene were also observed by Li et al. when studying the combustion of a larger char model ($C_{225}H_{182}N_4O_{36}S_3$) with ReaxFF and DFT.[68]

**Organic *S*-Dioxides.** *2H-thiopyran 1,1-Dioxide.* Among the studied *S*,*S*-dioxides **H** represents oxidized thioethers. They can eliminate sulfur as dioxide ($SO_2$). The reaction pathway found in the current work for **H** starts with an attack of an oxygen atom at the *S*,*S*-dioxide functionality (Figure 13), opening the ring and forming intermediate **H2** in a triplet state. This reaction is highly exothermic and shows no significant activation barrier. Reaction channel $\mathbf{R_H2}$ leads to the elimination of sulfur dioxide, requiring 39.1 kJ/mol of energy (Table 8).

*Sulfonyldibenzene.* Sulfones can connect two aromatic subsystems and are one of the main abundant exocyclic groups in (bio)char. While it was observed that **H** tends to eliminate sulfur dioxide ($SO_2$), in sulfonyldibenzene (**I**) sulfur leaves the organic framework in the mechanism shown in Figure 14 as sulfur monoxide (SO). The initial reaction steps take place at the carbon framework, starting with the addition of an HO· radical to one of the phenyl rings forming the reactive species **I2**. The sulfone functionality reacts by the insertion of oxygen into the C−S bond prior to the homolytical dissociation of the resulting S−O bond, forming **I3** and **I4**. Instead of a C−S bond dissociation, the sulfinyl group undergoes a rearrangement to an oxidanethione (compound **I5**). Eventually, sulfur monoxide **I6** can be eliminated with, however, a highly endothermic reaction energy of 202.4 kJ/mol (Table 9).

**Comparison of SFGs and OFGs.** Yönder et al.[19] investigated the reaction mechanisms of oxygen functional groups (OFGs) during char burnout applying the same automatized workflow[34] as used in the current work. Oxygen functionalities leave the carbon framework as $CO_xH_y$ species such as carbon dioxide, carbon monoxide, formic acid, and formaldehyde. Similar to sulfur, less oxidized OFGs are converted into highly oxidized groups that eliminate as carbon dioxide. Aromatic thiols undergo different reactions in the combustion atmosphere than the corresponding alcohols. For both functional groups, the initial reaction step is the abstraction of the terminal hydrogen atom, forming a radical center (Figure 15). In the case of aromatic alcohols, the radicals tend to react with the vicinal carbon atoms from the carbon framework, whereas in the case of thiols, the sulfur atom is oxidized in several steps, forming $SO_x$ volatiles.

**Rates for Oxidation versus Pyrolysis.** To the best of our knowledge, detailed kinetic data for the oxidation of SFGs in


https://doi.org/10.1021/acs.jpca.4c07973
J. Phys. Chem. A 2025, 129, 3300−3314

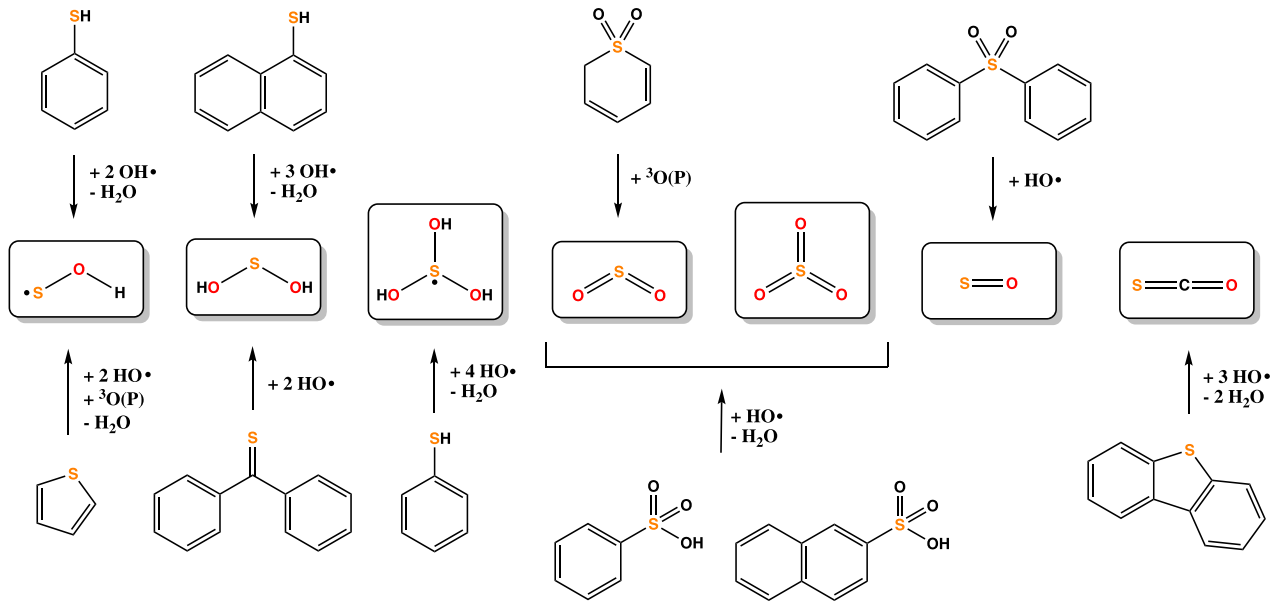



**Figure 18.** Overview of the elimination pathways of sulfur-containing leaving groups for different SFGs represented by compounds **A**–**I**.

aromatic hydrocarbons that could be directly compared with the current results is not yet available in the literature. For thiophene, Li et al.[84] studied possible pyrolysis reaction pathways and calculated rate constants based on transition state theory. Considering competing pathways during the combustion of thiophene functionalities, it is of interest to compare (see Figure 16) the pyrolysis pathways with the oxidation reactions found in the present work.

To compare the rates for these reactions, we recalculated the activation energies and kinetic parameters for the pyrolysis pathways reported by Li et al.[84] at the same level of theory used for all other reactions in the present work. Figure 17 shows a comparison of the rate constants for the initial pyrolysis reactions with those for the reaction steps $\mathbf{R_F2}$, $\mathbf{R_F3}$, and $\mathbf{R_F7}$ for the oxidation of thiophene (Figure 10). The reaction pathway for the oxidation involves HO· radicals for which concentrations as high as 10% (at atmospheric pressure) in all types of oxy-fuel flames were reported at elevated temperatures.[85] Also for thiophene, the oxidation starts in the presence of hydroxyl radicals with the addition of a HO· radical to the aromatic ring system (see $\mathbf{R_F1}$ in Figure 16). Since for oxy-fuel combustion processes hydroxyl radicals are a major species in the combustion atmosphere, the newly found reaction channels are important and should to be taken into account to model combustion under such conditions. The reaction channels found by Li et al.[84] for pyrolysis are in the range of 2000 K, nearly 3 orders of magnitude slower than the unimolecular rearrangement reactions in the reaction channel for oxidation, underlining that this channel becomes important when the partial pressure of HO· is sufficiently high. With decreasing temperature, the oxidation channel becomes increasingly more important, while for higher temperatures the pyrolysis channels gain importance.

## CONCLUSIONS

The aim of the current study has been to determine and analyze the most important reaction pathways for the initial oxidation steps of sulfur-containing functional groups during char during combustion. Sulfur exists in chars in the form of thiophenes, sulfur-(di)oxides, sulfonic acids, and thiol groups. To shed light on the reaction space of SFGs during char burnout, reactive MD simulations were done for each type of SFG to study the group-specific reaction behavior. Terminal as well as embedded S-containing groups react in the initial steps with HO· radicals or atomic oxygen ($^3$O(P)) forming $SO_xH_y$ species that can eliminate from the organic framework as volatiles. Moreover, we investigated how oxidation mechanisms vary with increasing system size, starting from benzene- to naphthalene-sized molecules. Figure 18 summarizes the initial elimination products of the studied SFG compounds **A**–**I**.

In aromatic thiols, the oxidation pathways lead to the elimination of $S(OH)_x$ species with $x$ = 1, 2, 3. For both, it was observed that sulfur is eliminated as sulfoxylic acid ($SO_2H_2$). For benzenethiol also, $H_3O_3S$· and HOS· were observed as leaving groups; elimination of the latter is, however, highly endothermic. The elimination can occur directly in the initial oxidation steps or after partial oxidation of the carbon framework. The mechanisms do not differ much between benzenethiol and naphthalenethiol. Hence, we conclude that the reactions of terminal thiol groups do not change much with the system size.

Sulfonic acids are decomposed in the combustion atmosphere by abstracting in an initial step the hydrogen atom from the R-$SO_3H$ group, leading to open-shell R-$SO_3$· radicals that can either eliminate sulfur trioxide or sulfur dioxide. The elimination of sulfur dioxide, yielding an aryl radical, is thermodynamically favored compared to the elimination of $SO_3$ which results in aryl radicals. Thiopyrane and diphenyl *S*,*S*-dioxides can connect two aromatic ring systems. In these compounds, sulfur leaves the carbon framework as SO and $SO_2$, respectively. Considering embedded functionalities, thiophenes are the only notable exception regarding the oxidation mechanism under increasing system sizes. It was found that sulfur is eliminated in thiophene as HOS·, which is initiated by HO· radicals. Embedding thiophenes into a larger aromatic system changes the reaction pathways because the vicinal carbon atoms of the former thiophene structure cannot be attacked directly by hydroxyl radicals. As a consequence, the sulfur atoms in nonembedded and embedded thiophenes are converted into different sulfur functionalities before leaving the carbon framework. In the case of dibenzothiophene, a thiopyran derivative is formed, which


https://doi.org/10.1021/acs.jpca.4c07973
J. Phys. Chem. A 2025, 129, 3300−3314

**Table 10. Rate Constant Parameters for the Modified Arrhenius Form, eq 5, for the Combustion Reactions of Compounds A–I**

| reaction | ln $A$ | $n$ | $E$ | units of $k(T)$ |
|---|---|---|---|---|
| A1 + HO· → A2 + $H_2O$ | barrierless | | | |
| A2 + HO· → A3 | barrierless | | | |
| A3 + HO· → A4 | barrierless | | | |
| A4 → A5 | 27.17 | 0.3128 | 3281.08 | 1/s |
| reverse | 31.22 | −0.0830 | 5211.55 | 1/s |
| A5 → A6 | barrierless | | | |
| A6 → A7 + Ph· | barrierless | | | |
| A5 + HO· → A8 + Ph· | 11.03 | 1.9552 | 8193.61 | $cm^3\ mol^{-1}\ s^{-1}$ |
| reverse | 4.61 | 2.1938 | 6704.51 | $cm^3\ mol^{-1}\ s^{-1}$ |
| A3 → A9 + Ph· | barrierless | | | |
| A1 + HO· → A10 | barrierless | | | |
| A1 + HO· → A11 + $H_2O$ | barrierless | | | |
| A1 + HO· → A12 + $H_2O$ | barrierless | | | |
| A1 + HO· → A13 + $H_2O$ | barrierless | | | |
| B1 + HO· → B2 + $H_2O$ | barrierless | | | |
| B2 → B3 | barrierless | | | |
| B3 + HO· → B4 | barrierless | | | |
| B4 → B5 + B6 | barrierless | | | |
| B3 + HO· → B7 | barrierless | | | |
| B7 + HO· → B8 | barrierless | | | |
| B8 → B6 + B9 | barrierless | | | |
| C1 + HO· → C2 + $H_2O$ | barrierless | | | |
| C2 → C3 + C4 | barrierless | | | |
| C2 → C5 + C6 | 25.76 | 0.4850 | 6705.83 | 1/s |
| reverse | 0.45 | 2.6437 | 15315.49 | $cm^3\ mol^{-1}\ s^{-1}$ |
| C2 → C7 | 24.21 | 0.7754 | 12433.59 | 1/s |
| reverse | 23.90 | 0.7584 | 10678.92 | 1/s |
| D1 + HO· → D2 + $H_2O$ | barrierless | | | |
| D2 → D3 + D4 | barrierless | | | |
| D2 → D5 + D6 | 27.35 | 0.2637 | 2537.66 | 1/s |
| reverse | 0.83 | 2.4875 | 15189.63 | $cm^3\ mol^{-1}\ s^{-1}$ |
| E1 + HO· → E2 | barrierless | | | |
| E2 + HO· → E3 | barrierless | | | |
| E3 → E4 | barrierless | | | |
| E3 → E10 + E11 | barrierless | | | |
| E4 + HO· → E5 + $H_2O$ | barrierless | | | |
| E5 → E6 | 28.90 | 0.1251 | 6374.52 | 1/s |
| reverse | 27.22 | 0.3119 | 3242.42 | 1/s |
| E6 → E7 | 24.02 | 0.6612 | 113.02 | 1/s |
| reverse | 25.24 | 0.5310 | 1472.04 | 1/s |
| E7 → E8 | 27.87 | 0.2378 | 227.52 | 1/s |
| reverse | 23.78 | 0.6719 | 19739.51 | 1/s |
| E8 → E9 + E10 | barrierless | | | |
| F1 → F2 | barrierless | | | |
| F2 → F3 | 29.46 | 0.0941 | 12290.08 | 1/s |
| reverse | 24.30 | 0.5391 | 4996.82 | 1/s |
| F3 → F4 | 27.70 | 0.4152 | 4434.00 | 1/s |
| reverse | 28.70 | 0.2459 | 7549.69 | 1/s |
| F4 → F5 | barrierless | | | |
| F5 → F6 | barrierless | | | |
| F6 → F7 | barrierless | | | |
| F7 → F8 + F9 | 35.50 | −0.4216 | 11366.79 | 1/s |
| reverse | 8.33 | 1.9527 | 1731.80 | $cm^3\ mol^{-1}\ s^{-1}$ |
| G1 + H· → G2 + $H_2$ | 18.42 | 1.8337 | 7342.21 | $cm^3\ mol^{-1}\ s^{-1}$ |
| reverse | 10.33 | 2.4481 | 2255.10 | $cm^3\ mol^{-1}\ s^{-1}$ |
| G1 + HO· → G2 + $H_2O$ | 10.97 | 2.3305 | 1114.02 | $cm^3\ mol^{-1}\ s^{-1}$ |
| reverse | 5.09 | 2.7641 | 3524.98 | $cm^3\ mol^{-1}\ s^{-1}$ |
| G1 → G2 + H· | | | | |
| G2 → G3 | 27.83 | 0.4583 | 30893.61 | 1/s |
| reverse | 29.12 | 0.1244 | 2114.32 | 1/s |



https://doi.org/10.1021/acs.jpca.4c07973
J. Phys. Chem. A 2025, 129, 3300−3314

Table 10. continued

| reaction | ln $A$ | $n$ | $E$ | units of $k(T)$ |
|---|---|---|---|---|
| G3 → G4 | 29.32 | 0.0950 | 2982.68 | 1/s |
| reverse | 27.43 | 0.2769 | 13113.97 | 1/s |
| G4 → G5 | 31.51 | 0.1659 | 18141.04 | 1/s |
| reverse | 26.05 | 0.4088 | 1988.53 | 1/s |
| G5 → G6 | 31.74 | −0.0922 | 8117.84 | 1/s |
| reverse | 25.72 | 0.4779 | 3393.83 | 1/s |
| G6 → G7 | 25.76 | 0.3907 | 3851.28 | 1/s |
| reverse | 30.95 | 0.0793 | 9960.61 | 1/s |
| G7 → G8 | 25.90 | 0.6806 | 24339.42 | 1/s |
| reverse | 26.17 | 0.6646 | 24599.33 | 1/s |
| G8 → G9 | 31.77 | −0.0868 | 17628.78 | 1/s |
| reverse | 31.74 | −0.0623 | 34658.92 | 1/s |
| G9 → G10 | 27.52 | 0.2703 | 24984.41 | 1/s |
| reverse | 28.99 | 0.2054 | 2546.40 | 1/s |
| G10 → G11 | 31.21 | 0.1382 | 20328.91 | 1/s |
| reverse | 22.87 | 0.7380 | 8182.75 | 1/s |
| G11 + HO· → G12 | barrierless | | | |
| G12 + HO· → G13 + $HO_2$· | barrierless | | | |
| G13 → G14 + G15 | barrierless | | | |
| H1 + $^3O(P)$ → H2 | barrierless | | | |
| H2 → H3 + H4 | barrierless | | | |
| I1 + HO· → I2 | barrierless | | | |
| I2 → I3 + I4 | 30.46 | 0.1723 | 32395.41 | 1/s |
| reverse | 5.92 | 1.8278 | 29789.54 | $cm^3\ mol^{-1}\ s^{-1}$ |
| I4 → I5 | 26.45 | 0.4907 | 26938.28 | 1/s |
| reverse | 25.90 | 0.6288 | 17709.74 | 1/s |
| I5 → I6 + Ph· | barrierless | | | |

reacts further to a thioketone. Sulfur is eventually eliminated as carbonyl sulfide (COS). Dibenzothiophene is the only system for which we observed that sulfur is eliminated as a carbon-bound species and not as $SO_x$ or $SO_xH_y$ species.

In addition to reaction and activation energies, we also computed rate constants for 300−3000 K, which, for a compact representation, were fitted to the modified Arrhenius form given in eq 5. The resulting kinetic parameters are listed in Table 10 of the Appendix. They can be used in future studies as input for, e.g., kinetic Monte Carlo approaches for sulfur-containing aromatic hydrocarbons and provide a starting point for extending combustion models of biomass-based or other solid fuels to account for the presence of sulfur-containing functional groups.

## APPENDIX A RATE CONSTANTS

## ASSOCIATED CONTENT

### Data Availability Statement

The DFT-optimized geometries along with the electronic energies of the reactants, products, and transition states of the studied reactions are available in a Zenodo repository[86] or on request from the authors.

## AUTHOR INFORMATION


### Corresponding Author

**Bastian Schnieder** − *Lehrstuhl für Theoretische Chemie I, D-44780 Bochum, Germany;* orcid.org/0009-0006-5847-6388; Phone: +49 (0)234 32 26846; Email: bastian.schnieder@ruhr-uni-bochum.de

### Authors

**Rochus Schmid** − *Computational Materials Chemistry Group, Ruhr-Universität Bochum, D-44780 Bochum, Germany;* orcid.org/0000-0002-1933-3644

**Christof Hättig** − *Lehrstuhl für Theoretische Chemie I, D-44780 Bochum, Germany;* orcid.org/0000-0002-5752-2710

Complete contact information is available at: https://pubs.acs.org/10.1021/acs.jpca.4c07973


### Author Contributions

B.S.: Investigation, conceptualization, methodology, validation, data curation, writing—original draft. R.S.: Supervision, project administration, funding acquisition, methodology, writing—review and editing. C.H.: Supervision, project administration, funding acquisition, conceptualization, methodology, validation, data curation, writing—review and editing.

### Notes

The authors declare no competing financial interest.

## ACKNOWLEDGMENTS

The authors thank the German Research Foundation (DFG) for funding this study within the framework of the SFB/Transregio 129 Oxyflame (Project number 215035359).

## REFERENCES

(1) Tapia, J. F. D.; Lee, J.-Y.; Ooi, R. E.; Foo, D. C.; Tan, R. R. A review of optimization and decision-making models for the planning of $CO_2$ capture, utilization and storage (CCUS) systems. *Sustainable Production and Consumption* **2018**, *13*, 1−15.

(2) Kätelhön, A.; Meys, R.; Deutz, S.; Suh, S.; Bardow, A. Climate change mitigation potential of carbon capture and utilization in the

chemical industry. *Proc. Natl. Acad. Sci. U. S. A.* **2019**, *116*, 11187−11194.
(3) Nath, F.; Mahmood, M. N.; Yousuf, N. Recent advances in CCUS: A critical review on technologies, regulatory aspects and economics. *Geoenergy Science and Engineering* **2024**, *238*, No. 212726.
(4) Harris, Z.; Spake, R.; Taylor, G. Land use change to bioenergy: A meta-analysis of soil carbon and GHG emissions. *Biomass and Bioenergy* **2015**, *82*, 27−39.
(5) Tanzer, S. E.; Ramírez, A. When are negative emissions negative emissions? *Energy Environ. Sci.* **2019**, *12*, 1210−1218.
(6) Pelissari, M. R.; San Martín Cañas, S.; Ciotta, M. R.; Tassinari, C. C. G. In BECCUS: a digital approach for a bioethanol plant in Brazil, Rio Oil & Gas Expo and Conference, **2020**.
(7) Rogieri Pelissari, M.; Gomes Relva, S.; Peyerl, D. *Energy Transition in Brazil*; Peyerl, D.; Relva, S.; Da Silva, V., Eds.; Springer Nature Switzerland: Cham, 2023; pp 141−157.
(8) Janu, R.; Mrlik, V.; Ribitsch, D.; Hofman, J.; Sedláček, P.; Bielská, L.; Soja, G. Biochar surface functional groups as affected by biomass feedstock, biochar composition and pyrolysis temperature. *Carbon Resources Conversion* **2021**, *4*, 36−46.
(9) Naeem, M.; Khalid, M.; Arshad, M.; Ahmad, R. Yield and nutrient composition of biochar produced from different feedstocks at varying pyrolytic temperatures. *Pak. J. Agric. Res.* **2014**, *51*, 75−82.
(10) Choudhary, T. K.; Khan, K. S.; Hussain, Q.; Ahmad, M.; Ashfaq, M. Feedstock-induced changes in composition and stability of biochar derived from different agricultural wastes. *Arab. J. Geosci.* **2019**, *12*, 617.
(11) Li, S.; Harris, S.; Anandhi, A.; Chen, G. Predicting biochar properties and functions based on feedstock and pyrolysis temperature: A review and data syntheses. *Journal of Cleaner Production* **2019**, *215*, 890−902.
(12) Al-Wabel, M. I.; Al-Omran, A.; El-Naggar, A. H.; Nadeem, M.; Usman, A. R. Pyrolysis temperature induced changes in characteristics and chemical composition of biochar produced from conocarpus wastes. *Bioresour. Technol.* **2013**, *131*, 374−379.
(13) Tomczyk, A.; Sokołowska, Z.; Boguta, P. Biochar physicochemical properties: pyrolysis temperature and feedstock kind effects. *Reviews in Environmental Science and Bio/Technology* **2020**, *19*, 191−215.
(14) Cheah, S.; Malone, S. C.; Feik, C. J. Speciation of Sulfur in Biochar Produced from Pyrolysis and Gasification of Oak and Corn Stover. *Environ. Sci. Technol.* **2014**, *48*, 8474−8480.
(15) Li, B.; Liu, D.; Lin, D.; Xie, X.; Wang, S.; Xu, H.; Wang, J.; Huang, Y.; Zhang, S.; Hu, X. Changes in Biochar Functional Groups and Its Reactivity after Volatile Char Interactions during Biomass Pyrolysis. *Energy Fuels* **2020**, *34*, 14291−14299.
(16) Li, P.; Wan, K.; Chen, H.; Zheng, F.; Zhang, Z.; Niu, B.; Zhang, Y.; Long, D. Value-Added Products from Catalytic Pyrolysis of Lignocellulosic Biomass and Waste Plastics over Biochar-Based Catalyst: A State-of-the-Art Review. *Catalysts* **2022**, *12*, 1067.
(17) Locaspi, A.; Debiagi, P.; Pelucchi, M.; Hasse, C.; Faravelli, T. A Predictive Physico-chemical Model of Biochar Oxidation. *Energy Fuels* **2021**, *35*, 14894−14912.
(18) Tian, H.; He, Z.; Wang, J.; Jiao, H.; Hu, Z.; Yang, Y. Density Functional Theory Study on the Mechanism of Biochar Gasification in $CO_2$ Environment. *Ind. Eng. Chem. Res.* **2020**, *59*, 19972−19981.
(19) Yönder, O.; Schmitz, G.; Schmid, R.; Schnieder, B.; Hättig, C. A computational chemistry study on the evolution of oxygen functional groups during char burnout. *Fuel* **2024**, *365*, No. 131217.
(20) https://zenodo.org/doi/10.5281/zenodo.10514181 (accessed October, 2024).
(21) Leng, L.; Liu, R.; Xu, S.; Mohamed, B. A.; Yang, Z.; Hu, Y.; Chen, J.; Zhao, S.; Wu, Z.; Peng, H.; et al. An overview of sulfur-functional groups in biochar from pyrolysis of biomass. *Journal of Environmental Chemical Engineering* **2022**, *10*, No. 107185.
(22) Chen, H.; Li, B.; Yang, J.; Zhang, B. Transformation of sulfur during pyrolysis and hydropyrolysis of coal. *Fuel* **1998**, *77*, 487−493.
(23) Hu, H.; Fang, Y.; Liu, H.; Yu, R.; Luo, G.; Liu, W.; Li, A.; Yao, H. The fate of sulfur during rapid pyrolysis of scrap tires. *Chemosphere* **2014**, *97*, 102−107.
(24) Nemitallah, M. A.; Habib, M. A.; Badr, H. M.; Said, S. A.; Jamal, A.; Ben-Mansour, R.; Mokheimer, E. M. A.; Mezghani, K. Oxy-fuel combustion technology: current status, applications, and trends. *International Journal of Energy Research* **2017**, *41*, 1670−1708.
(25) Scheffknecht, G.; Al-Makhadmeh, L.; Schnell, U.; Maier, J. Oxy-fuel coal combustion-A review of the current state-of-the-art. *International Journal of Greenhouse Gas Control* **2011**, *5*, S16−S35.
(26) Huang, Y.; Cannon, F. S.; Watson, J. K.; Reznik, B.; Mathews, J. P. Activated carbon efficient atomistic model construction that depicts experimentally-determined characteristics. *Carbon* **2015**, *83*, 1−14.
(27) Chacón, F.; Cayuela, M. L.; Roig, A.; Sánchez-Monedero, M. Understanding, measuring and tuning the electrochemical properties of biochar for environmental applications. *Reviews in Environmental Science and Bio/Technology* **2017**, *16*, 695−715.
(28) Chen, Y.; Zhang, X.; Chen, W.; Yang, H.; Chen, H. The structure evolution of biochar from biomass pyrolysis and its correlation with gas pollutant adsorption performance. *Bioresour. Technol.* **2017**, *246*, 101−109.
(29) Chen, X.; Zhang, L.; Xu, W.; Ding, X.; Chen, S.; She, X.; Guo, X.; Dong, C.-L.; Huang, Y.; Zhang, L.; et al. Biochar aerogel decorated with thiophene S manipulated 5-membered rings boosts nitrogen fixation. *Applied Catalysis B: Environmental* **2022**, *313*, No. 121425.
(30) Menéndez-Díaz, J.; Martín-Gullón, I. *Activated Carbon Surfaces in Environmental Remediation*; Bandosz, T. J., Ed.; Interface Science and Technology; Elsevier, 2006; Vol. 7, pp 1−47.
(31) Maffei, T.; Sommariva, S.; Ranzi, E.; Faravelli, T. A predictive kinetic model of sulfur release from coal. *Fuel* **2012**, *91*, 213−223.
(32) Yönder, O.; Schmitz, G.; Hättig, C.; Schmid, R.; Debiagi, P.; Hasse, C.; Locaspi, A.; Faravelli, T. Can Small Polyaromatics Describe Their Larger Counterparts for Local Reactions? A Computational Study on the H-Abstraction Reaction by an H-Atom from Polyaromatics. *J. Phys. Chem. A* **2020**, *124*, 9626−9637.
(33) van Duin, A. C. T.; Dasgupta, S.; Lorant, F.; Goddard, W. A. ReaxFF: A Reactive Force Field for Hydrocarbons. *J. Phys. Chem. A* **2001**, *105*, 9396−9409.
(34) Schmitz, G.; Yönder, O.; Schnieder, B.; Schmid, R.; Hättig, C. An automatized workflow from molecular dynamic simulation to quantum chemical methods to identify elementary reactions and compute reaction constants. *J. Comput. Chem.* **2021**, *42*, 2264−2282.
(35) Schmid, R. *pylmps*, 2024. https://github.com/MOFplus/pylmps.git (accessed October, 2024).
(36) Thompson, A. P.; Aktulga, H. M.; Berger, R.; Bolintineanu, D. S.; Brown, W. M.; Crozier, P. S.; in't Veld, P. J.; Kohlmeyer, A.; Moore, S. G.; Nguyen, T. D.; et al. LAMMPS - a flexible simulation tool for particle-based materials modeling at the atomic, meso, and continuum scales. *Comput. Phys. Commun.* **2022**, *271*, No. 108171.
(37) Weismiller, M. R.; van Duin, A. C. T.; Lee, J.; Yetter, R. A. ReaxFF Reactive Force Field Development and Applications for Molecular Dynamics Simulations of Ammonia Borane Dehydrogenation and Combustion. *J. Phys. Chem. A* **2010**, *114*, 5485−5492.
(38) Smith, R. Role of hydroxyl radicals in combustion. *Coal Res. CSIRO* **1967**, *32*, 9−18.
(39) He, G.; Ma, J.; Chu, B.; Hu, R.; Li, H.; Gao, M.; Liu, Y.; Wang, Y.; Ma, Q.; Xie, P.; et al. Generation and Release of OH Radicals from the Reaction of $H_2O$ with $O_2$ over Soot. *Angew. Chem., Int. Ed.* **2022**, *61*, No. e202201638.
(40) Hayden, T. R. S.; Malarich, N.; Petrykowski, D.; Nigam, S. P.; Christopher, J. D.; Lapointe, C.; Wimer, N. T.; Hamlington, P. E.; Rieker, G. B. OH radical measurements in combustion environments using wavelength modulation spectroscopy and dual-frequency comb spectroscopy near 1491 nm. *Appl. Phys. B: Lasers Opt.* **2019**, *125*, 226.
(41) Balasubramani, S. G.; Chen, G. P.; Coriani, S.; Diedenhofen, M.; Frank, M. S.; Franzke, Y. J.; Furche, F.; Grotjahn, R.; Harding, M. E.; Hättig, C.; et al. TURBOMOLE: Modular program suite for ab initio quantum-chemical and condensed-matter simulations. *J. Chem. Phys.* **2020**, *152*, 184107.
(42) *TURBOMOLE V7.6, a development of University of Karlsruhe and Forschungszentrum Karlsruhe GmbH, 1989−2007, TURBOMOLE GmbH, since 2007*. http://www.turbomole.com.

(43) Eichkorn, K.; Treutler, O.; Öhm, H.; Häser, M.; Ahlrichs, R. Auxiliary basis sets to approximate Coulomb potentials (Chem. Phys. Letters 240 (1995) 283-290). *Chem. Phys. Lett.* **1995**, *242*, 652−660.
(44) Eichkorn, K.; Weigend, F.; Treutler, O.; Ahlrichs, R. Auxiliary basis sets for main row atoms and transition metals and their use to approximate Coulomb potentials. *Theor. Chem. Acc.* **1997**, *97*, 119−124.
(45) Grimme, S.; Antony, J.; Ehrlich, S.; Krieg, H. A consistent and accurate ab initio parametrization of density functional dispersion correction (DFT-D) for the 94 elements H-Pu. *J. Chem. Phys.* **2010**, *132*, 154104.
(46) Tao, J.; Perdew, J. P.; Staroverov, V. N.; Scuseria, G. E. Climbing the Density Functional Ladder: Nonempirical Meta−Generalized Gradient Approximation Designed for Molecules and Solids. *Phys. Rev. Lett.* **2003**, *91*, No. 146401.
(47) Schäfer, A.; Horn, H.; Ahlrichs, R. Fully optimized contracted Gaussian basis sets for atoms Li to Kr. *J. Chem. Phys.* **1992**, *97*, 2571−2577.
(48) Staroverov, V. N.; Scuseria, G. E.; Tao, J.; Perdew, J. P. Comparative assessment of a new nonempirical density functional: Molecules and hydrogen-bonded complexes. *J. Chem. Phys.* **2003**, *119*, 12129−12137.
(49) Schäfer, A.; Huber, C.; Ahlrichs, R. Fully optimized contracted Gaussian basis sets of triple zeta valence quality for atoms Li to Kr. *J. Chem. Phys.* **1994**, *100*, 5829−5835.
(50) Csonka, G. I.; Ruzsinszky, A.; Perdew, J. P. Estimation, Computation, and Experimental Correction of Molecular Zero-Point Vibrational Energies. *J. Phys. Chem. A* **2005**, *109*, 6779−6789.
(51) Hättig, C.; Tew, D. P.; Köhn, A. Communications: Accurate and efficient approximations to explicitly correlated coupled-cluster singles and doubles, CCSD-F12. *J. Chem. Phys.* **2010**, *132*, 231102.
(52) Peterson, K. A.; Adler, T. B.; Werner, H.-J. Systematically convergent basis sets for explicitly correlated wavefunctions: The atoms H, He, B−Ne, and Al−Ar. *J. Chem. Phys.* **2008**, *128*, No. 084102.
(53) Hättig, C. Optimization of auxiliary basis sets for RI-MP2 and RI-CC2 calculations: Core-valence and quintuple-$\zeta$ basis sets for H to Ar and QZVPP basis sets for Li to Kr. *Phys. Chem. Chem. Phys.* **2005**, *7*, 59−66.
(54) Weigend, F.; Köhn, A.; Hättig, C. Efficient use of the correlation consistent basis sets in resolution of the identity MP2 calculations. *J. Chem. Phys.* **2002**, *116*, 3175−3183.
(55) Yousaf, K. E.; Peterson, K. A. Optimized auxiliary basis sets for explicitly correlated methods. *J. Chem. Phys.* **2008**, *129*, 184108.
(56) Häser, M.; Ahlrichs, R. Improvements on the direct SCF method. *J. Comput. Chem.* **1989**, *10*, 104−111.
(57) Halgren, T. A.; Lipscomb, W. N. The synchronous-transit method for determining reaction pathways and locating molecular transition states. *Chem. Phys. Lett.* **1977**, *49*, 225−232.
(58) Elber, R.; Karplus, M. A method for determining reaction paths in large molecules: Application to myoglobin. *Chem. Phys. Lett.* **1987**, *139*, 375−380.
(59) Mills, G.; Jónsson, H. Quantum and thermal effects in $H_2$ dissociative adsorption: Evaluation of free energy barriers in multi-dimensional quantum systems. *Phys. Rev. Lett.* **1994**, *72*, 1124−1127.
(60) Helgaker, T. Transition-state optimizations by trust-region image minimization. *Chem. Phys. Lett.* **1991**, *182*, 503−510.
(61) Grimme, S. Supramolecular Binding Thermodynamics by Dispersion-Corrected Density Functional Theory. *Chem.—Eur. J.* **2012**, *18*, 9955−9964.
(62) Shavitt, I. A Calculation of the Rates of the Ortho-Para Conversions and Isotope Exchanges in Hydrogen. *J. Chem. Phys.* **1959**, *31*, 1359−1367.
(63) Kee, R. J.; Rupley, F. M.; Miller, J. A. *Chemkin-II: A Fortran chemical kinetics package for the analysis of gas-phase chemical kinetics*; Sandia National Lab. (SNL-CA): Livermore, 1989.
(64) Döntgen, M.; Schmalz, F.; Kopp, W. A.; Kröger, L. C.; Leonhard, K. Automated Chemical Kinetic Modeling via Hybrid Reactive Molecular Dynamics and Quantum Chemistry Simulations. *J. Chem. Inf. Model.* **2018**, *58*, 1343−1355.
(65) Hellwich, K.-H.; Hartshorn, R. M.; Yerin, A.; Damhus, T.; Hutton, A. T. Brief guide to the nomenclature of organic chemistry (IUPAC Technical Report). *Pure Appl. Chem.* **2020**, *92*, 527−539.
(66) Johnson, D. E. Pyrolysis of benzenethiol. *Fuel* **1987**, *66*, 255−260.
(67) Al-Muhtaseb, A. H.; Altarawneh, M.; Almatarneh, M. H.; Poirier, R. A.; Assaf, N. W. Theoretical study on the unimolecular decomposition of thiophenol. *J. Comput. Chem.* **2011**, *32*, 2708−2715.
(68) Li, G.-Y.; Wang, F.; Wang, J.-P.; Li, Y.-Y.; Li, A.-Q.; Liang, Y.-H. ReaxFF and DFT study on the sulfur transformation mechanism during the oxidation process of lignite. *Fuel* **2016**, *181*, 238−247.
(69) Ventura, O. N.; Segovia, M.; Vega-Teijido, M.; Katz, A.; Kieninger, M.; Tasinato, N.; Salta, Z. Correcting the Experimental Enthalpies of Formation of Some Members of the Biologically Significant Sulfenic Acids Family. *J. Phys. Chem. A* **2022**, *126*, 6091−6109.
(70) Makarov, S. V.; Horváth, A. K.; Makarova, A. S. Reactivity of Small Oxoacids of Sulfur. *Molecules* **2019**, *24*, 2768.
(71) Zaman, A. C. Pyrolysis of sulfonic acid substituted benzenes and investigation of $CO_2$ capture capability of resulting carbons. *J. Solid State Chem.* **2021**, *303*, No. 122546.
(72) Hindiyarti, L.; Glarborg, P.; Marshall, P. Reactions of SO3 with the O/H Radical Pool under Combustion Conditions. *J. Phys. Chem. A* **2007**, *111*, 3984−3991.
(73) Goldman, M. J.; Green, W. H.; Kroll, J. H. Chemistry of Simple Organic Peroxy Radicals under Atmospheric through Combustion Conditions: Role of Temperature, Pressure, and NOx Level. *J. Phys. Chem. A* **2021**, *125*, 10303−10314.
(74) Suh, I.; Zhang, R.; Molina, L. T.; Molina, M. J. Oxidation Mechanism of Aromatic Peroxy and Bicyclic Radicals from OH-Toluene Reactions. *J. Am. Chem. Soc.* **2003**, *125*, 12655−12665.
(75) Zhang, Y.; Sun, J.; Sun, Y.; Tang, Y.; Wang, R. Mechanistic and kinetic study on the reaction of thiophene with hydroxyl radical. *Computational and Theoretical Chemistry* **2016**, *1092*, 74−81.
(76) Atkinson, R.; Aschmann, S. M.; Carter, W. P. L. Kinetics of the reactions of $O_3$ and OH radicals with furan and thiophene at 298 ± 2 K. *International Journal of Chemical Kinetics* **1983**, *15*, 51−61.
(77) Lee, J. H.; Tang, I. N. Absolute rate constants for the hydroxyl radical reactions with ethane, furan, and thiophene at room temperature. *J. Chem. Phys.* **1982**, *77*, 4459−4463.
(78) Ling, L.-X.; Zhang, R.-G.; Wang, B.-J.; Xie, K.-C. Density functional theory study on the pyrolysis mechanism of thiophene in coal. *Journal of Molecular Structure: THEOCHEM* **2009**, *905*, 8−12.
(79) Liu, J.; Fan, X.-R.; Zhao, W.; Yang, S.-W.; Hu, B.; Yang, S.-G.; Lu, Q. Mechanical insight into the formation of $H_2S$ from thiophene pyrolysis: The influence of $H_2O$. *Chemosphere* **2021**, *279*, No. 130628.
(80) Li, T.; Li, J.; Zhang, H.; Sun, K.; Xiao, J. DFT Research on Benzothiophene Pyrolysis Reaction Mechanism. *J. Phys. Chem. A* **2019**, *123*, 796−810.
(81) Li, T.; Li, J.; Zhang, H.; Sun, K.; Xiao, J. DFT Study on the Dibenzothiophene Pyrolysis Mechanism in Petroleum. *Energy Fuels* **2019**, *33*, 8876−8895.
(82) Dartiguelongue, C.; Behar, F.; Budzinski, H.; Scacchi, G.; Marquaire, P. Thermal stability of dibenzothiophene in closed system pyrolysis: Experimental study and kinetic modelling. *Org. Geochem.* **2006**, *37*, 98−116.
(83) Ryabova, V.; Ignatovich, L. *Thiophenes*; Joule, J. A., Ed.; Springer International Publishing: Cham, 2015; pp 43−108.
(84) Li, T.; Zhang, H.; Li, Y.; Li, J.; Wang, J.; Xiao, J. Theoretical Study on the Unimolecular Pyrolysis of Thiophene and Modeling. *ACS Omega* **2021**, *6*, 20471−20482.
(85) Linow, S.; Dreizler, A.; Janicka, J.; Hassel, E. P. Measurement of temperature and concentration in oxy-fuel flames by Raman/Rayleigh spectroscopy. *Measurement Science and Technology* **2002**, *13*, 1952.
(86) Schnieder, B.; Hättig, C.; Schmid, R. Raw data to "A Quantum Chemical Study on the Evolution of Sulfur Functional Groups During Char Burnout", 2024. https://doi.org/10.5281/zenodo.10780997 (accessed January, 2025).